Applied Catalysis B: Environmental 301 (2022) 120826

Contents lists available at ScienceDirect

Applied Catalysis B: Environmental

journal homepage: www.elsevier.com/locate/apcatb

Defect-rich graphene stabilized atomically dispersed Cu_3 clusters with enhanced oxidase-like activity for antibacterial applications

FanChi Meng [a,b,1], Mi Peng [c,1], Yunlei Chen [d,1], Xiangbin Cai [f,1], Fei Huang [b], Lini Yang [a,*], Xiao Liu [a], Tao Li [a], Xiaodong Wen [d,e], Ning Wang [f], Dequan Xiao [g], Hong Jiang [c], Lixin Xia [a,*], Hongyang Liu [b,*], Ding Ma [c,*]

[a] Department of Chemistry, Liaoning University, 66 Congshan Road, Shenyang, Liaoning 110036, China
[b] Shenyang National Laboratory for Materials Science, Institute of Metal Research, Chinese Academy of Sciences, Shenyang 110016, PR China
[c] Beijing National Laboratory for Molecular Sciences, College of Chemistry and Molecular Engineering and College of Engineering, and BIC-ESAT, Peking University, Beijing 100871, PR China
[d] State Key Laboratory of Coal Conversion, Institute Coal Chemistry, Chinese Academy of Sciences, Taiyuan 030001, PR China
[e] University of Chinese Academy of Science, No. 19A Yuanquan Road, Beijing 100049, PR China
[f] Department of Physics and Center for Quantum Materials, Hong Kong University of Science and Technology, Clear Water Bay, Kowloon, Hong Kong, SAR, PR China
[g] Center for Integrative Materials Discovery, Department of Chemistry and Chemical Engineering, University of New Haven, 300 Boston Post Road, West Haven, Connecticut 06516, United States

ARTICLE INFO

Keywords:
Atomic dispersion
Cu cluster
Defect-rich graphene
Oxidase-like activity
Antibacterial

ABSTRACT

Nanozyme has attracted great attention due to its diverse enzymatic catalytic activities. But there are still challenges in constructing novel nanozyme with robust catalytic activity. Here, we report an atomically dispersed and fully exposed Cu_3 cluster stabilized on defect-rich nanodiamond-graphene hybrid support (Cu_3/ND@G) with unique active adsorption sites, which benefit the adsorption and cleavage of O_2, resulting in enhanced oxidase-like and antibacterial activity. The catalytic rate constant of Cu_3/ND@G ($K_{cat} = 1.474 \times 10^{-1}$ s^{-1}) is higher than those of previously reported copper single atom oxidase mimics (0.5×10^{-3} s^{-1}) and even the commercial Pt/C mimics (1.01×10^{-2} s^{-1}). DFT calculation revealed that the atomically dispersed Cu_3 cluster as active center significantly improves the oxidase-like activity, attributing to the easy dissociation of O_2 into reactive oxygen species (•OH). The atomically dispersed Cu_3 cluster with an antibacterial rate of 100% in the NaAc buffer presents its potential application in the field of antibacterial materials.

1. Introduction

Nanozyme, a class of nanomaterials with enzyme-like catalytic activity, has received increasing attention due to the advantages of high stability and low-cost. Since its report in 2007 [1], nanozyme has been widely studied as a simple and efficient alternative material for natural enzymes, with wide applications in biosensing, immunoassay and disease therapy fields [2–5]. Recently, different materials have been studied as nanozyme, such as metal oxides, noble metals, and nanocarbon materials [6–12]. However, traditional nanozymes face challenges due to their low catalytic activity and difficulty to tailoring catalytic active sites.

The discovery of single-atom nanozyme has further attracted great attention [13–18]. The atomically dispersed metal active sites maximize the utilization of metal atoms, leading to high catalytic activity and metal usage efficiency of the material. Importantly, the coordination structure of isolated metal atoms can be precisely designed and controlled. Thus, the electronic structure and coordination geometry of catalytic active centers can be well depicted, which helps the understanding of the structure-performance correlation of nanozyme [19]. However, single-atom catalysts may encounter low catalytic efficiency and sintering due to the lack of neighboring sites in some reactions. Compared with single atom catalysts, a type of atomically dispersed and fully exposed cluster catalysts (FECC) was proposed, which can not only provide adjacent metal atoms as catalytic sites but also maintain full atomic utilization efficiency, offering a variety of structural possibilities

* Corresponding authors.
E-mail addresses: lnyang@lnu.edu.cn (L. Yang), lixinxia@lnu.edu.cn (L. Xia), liuhy@imr.ac.cn (H. Liu), dma@pku.edu.cn (D. Ma).
[1] These authors contributed equally to this work.

https://doi.org/10.1016/j.apcatb.2021.120826
Received 11 June 2021; Received in revised form 8 August 2021; Accepted 28 August 2021
Available online 14 October 2021

and catalytic feasibilities [20–22]. Some atomically dispersed and fully exposed cluster catalysts can show the enzyme-like activity and thus have potential application in the field of nanozyme.

Here, in this paper, we report an atomically dispersed and fully exposed Cu cluster with an average of three Cu atoms stabilized on nanodiamond-graphene (ND@G) hybrid support with excellent oxidase-like activity (Cu_3/ND@G). The employed ND@G support features a nanodiamond core and curved graphene shells decorated with abundant defects formed during the annealing of commercial nanodiamond, which can anchor various metal species through the construction of metal-carbon bonds between the defective graphene surface and metal atoms [23,24]. The as-prepared Cu_3/ND@G with atomically dispersed and fully exposed Cu_3 cluster could maximum atomic utilization efficiency and thus the oxidase-like activity. The catalytic rate constant of Cu_3/ND@G is much higher than that of reported copper-based oxidase mimics and is even 15 times higher than that of commercial Pt/C mimics. DFT calculations and 3, 3′, 5, 5′-tetramethylbenzidine (TMB) oxidation experiment both revealed that the atomically dispersed and fully dispersed Cu_3 cluster as active center significantly improved the oxidase-like activity of nanozyme, due to the easy dissociation of oxygen into reactive oxygen species (•OH) in the NaAc buffer (pH = 4.5) [25–27]. The generated oxygen species can avidly bind with protein, lipid, polysaccharide, and bacteria membrane, resulting in perforation of bacterial membrane and subsequent cell death [28–30]. The plate count experiment of the Cu_3/ND@G against *Escherichia coli* (*E. coli*) indicated that Cu_3/ND@G possesses robust antibacterial properties, in comparison with that of ND@G supported Cu nanoparticles (Cu-NPs/ND@G). The present work paves a new way for designing novel atomically dispersed metal-cluster catalysts with potential applications as efficient antibacterial materials.

2. Experimental

2.1. Materials

Nanodiamond (ND) was purchased from Beijing Grish Hitech Co., Ltd, China. Copper nitrate trihydrate ($Cu(NO_3)_2$•3 H_2O) was obtained from An Naiji Chemical. Agar powder, tryptone, and yeast extract powder were provided by Aladdin Chemical. All the chemicals used in this research are in analytic grade. Gram-negative bacteria: Escherichia coli was selected as reference strains.

2.2. Synthesis of ND@G

ND@G was prepared by treating the commercial nanodiamond powder at 1100 ℃ under Ar atmosphere for 4 h, following by further purified with hydrochloric acid for 24 h, then the obtained samples were washed with deionized water. Finally, the ND@G was obtained after drying in vacuum.

2.3. Synthesis of Cu-NPs/ND@G

The Cu-NPs/ND@G with 0.5 wt% loading was prepared by the traditional wetness impregnation method. The ND@G (200 mg) powders were added into 20 mL anhydrous ethanol; then, $Cu(NO_3)_2$•3 H_2O (3.8 mg) was dissolved in 0.2 mL anhydrous ethanol and mixed with the graphene solution heated at 25 ℃ with magnetically stirring overnight, and finally dried at 60 ℃. The prepared materials were reduced in H_2 at 200 ℃ with a holding time of 1 h to yield the Cu-NPs/ND@G composite material. The obtained Cu-NPs/ND@G was characterized by HAADF-STEM.

2.4. Synthesis of Cu_3/ND@G

The Cu_3/ND@G nanozyme with 0.5 wt% loading was prepared through a conventional deposition-precipitation method. The ND@G (200 mg) powders were added into 30 mL deionized water and sonicate to disperse it. Then, the pH of the mixture was adjusted to 11 with a 0.25 M Na_2CO_3 solution. Afterwards, $Cu(NO_3)_2$•3 H_2O (3.8 mg) was dissolved in 5 mL deionized water and mixed with the ND@G suspension heated at 100 ℃ with magnetically stirring for 1 h. Finally, the black precipitate was collected, washed three times using deionized water and dried in vacuum at 60 ℃ for 12 h. The prepared materials were reduced in H_2 at 600 ℃ with a holding time of 1 h to yield the Cu_3/ND@G composite material.

2.5. Characterization

The aberration-corrected high-angle annular dark-field scanning transmission electron microscopy (AC-HAADF-STEM) images were taken by a JEOL JEM ARM 200CF aberration-corrected cold field-emission scanning transmission electron microscope of 200 kV. Raman spectra were acquired using a LabRam HR800 at a 532 nm excitation. The XRD patterns were obtained on a Bruker Smart APEX II powder diffractometer operated at 40 KV and 200 mA with Cu Kα radiation. The X-ray photoelectron spectroscopy (XPS) was performed by ESCALAB 250 instrument with a monochromatic Al Kα source (1489.6 eV, 150 W, 50.0 eV pass energy). The XAFS measurements were carried out in Shanghai Synchroton Radiation Facility (SSRF). Electron spin resonance (ESR) spectra were obtained by using JES-X320 ESR spectrometer. The transmission electron microscopy (TEM) images were taken by a FEI Tecnai G2 F20 model instrument to observe bacterials morphology. The samples were prepared by dropping the bacterials suspension on the copper mesh.

2.6. Oxidase-like activity

To study the oxidase-like activity of Cu-NPs/ND@G and Cu_3/ND@G nanozyme, the steadystate kinetic assays were carried out using TMB as substrates at room temperature. The nanozyme and TMB were added to 1 mL NaAc buffer (pH = 4.5), then the mixture was put at room temperature with a holding time of 10 min. Next, the oxidase-like activity of nanozyme was studied by measuring the change of UV absorption at 652 nm using a UV spectrophotometer. The final working concentrations were 0.1 mg mL^{-1} for Cu-NPs/ND@G and Cu_3/ND@G nanozyme, and the control experiments were carried out at final working concentrations were 600 μM for TMB. All the procedures were repeated three times. The Michaelis-Menten constant was calculated by equation: $V_0 = V_{max} \times [S] / (K_m + [S])$, where V_0 is the initial velocity, V_{max} is the maximum reaction velocity, [S] is the substrate concentration, and K_m is the Michaelis constant. The catalytic rate constant $K_{cat} = V_{max} / [E]$ was calculated, where [E] is the molar concentration of metal in nanozyme.

2.7. Detection of hydroxyl radical (•OH)

The generation of •OH was evaluated by ESR spectrometer using DMPO spin-trapping adduct (DMPO: 5, 5′-dimethyl-1-pyrroline N-oxide). During the experiment, the solutions include (a) 200 μg mL^{-1} Cu_3/ND@G/20 mM DMPO; (b) 200 μg mL^{-1} Cu-NPs/ND@G/20 mM DMPO. All mixtures were dispersed in pH 4.5 NaAc buffer (0.2 M). After reacting at room temperature and air for 10 min, the solutions were then aspirated into quartz capillaries for ESR analysis.

2.8. Antibacterial properties test

The antibacterial activity of Cu-NPs/ND@G or Cu_3/ND@G nanozyme was evaluated by the plate count method. The gram-negative *Escherichia coli* were diluted with NaAc buffer (pH = 4.5) to 1×10^4 CFU/mL. Then, the nanozyme was added to the bacterial suspension (The final working concentrations were 0.1 mg mL^{-1}), and 100 μL of this bacterial suspension was evenly spread over the surface of the Luria-Bertani (LB) medium. Finally, the medium was placed in a constant

temperature incubator at 37 ℃ overnight. The antibacterial activity was evaluated by counting colonies.

2.9. Computational details

All calculations were performed using the plane-wave based DFT method implemented in the Vienna Ab Initio Simulation Package (VASP) [31,32]. We described the electron-ion interaction using the projector augmented wave (PAW) method [33,34]. The generalized gradient approximation and the Perdew-Burke-Ernzerhof functional (GGA-PBE) describe the exchange and correlation energies for all systems [35]. The plane wave expansion of the wave functions adopted an energy cut-off of 400 eV. The ground-state structure of bulk and surfaces were obtained by minimizing forces with the conjugate-gradient algorithm until the force on each ion is below 0.03 eV/Å and the convergence criteria for electronic self-consistent interactions is 10^{-5}. Cu_3 cluster embedded into a monovacancy at 5 × 5 super cell of graphene was adopted as model to simulate the active site of O_2 activation (Cu_3OH@Gr) through comparative investigation between potential Cu_3 cluster models and EXAFS data. The vacuum layer was set to 20 Å to avoid interaction from adjacent cells. The Monkhorst-Pack k-point set to 2 × 2 × 1 in the reciprocal lattice, and the electronic occupancies were determined according to the Gaussian smearing method with σ = 0.1 eV. Spin-polarized calculations have been performed. The most stable configurations of the reactants and intermediates on Cu_3OH@Gr were obtained by the standard minimization of DFT.

3. Results and discussion

3.1. Construction of atomically dispersed and fully exposed Cu_3-cluster nanozyme

The detailed structures of Cu-NPs/ND@G and Cu_3/ND@G were determined by aberration-corrected high-angle annular dark-field scanning transmission electron microscopy (AC-HAADF-STEM). Fig. 1A shows that the Cu-NPs with sizes ranging from 2 to 3 nm are uniformly distributed on the ND@G surface (Fig. S2). The image in Fig. 1B shows that the obtained Cu-NPs are single nanocrystals with the lattice fringes of Cu (d = 0.208 nm) corresponding to the standard Cu (111) plane. To improve the oxidase-like activity and enhance the atomic utilization efficiency, the Cu_3/ND@G was prepared through a conventional deposition-precipitation method. As seen in Fig. 1C and D, the bright spots present the atomically dispersed Cu_3 cluster sites. The AC-HAADF-STEM images of Cu_3/ND@G strongly evidenced the formation of fully exposed and atomically dispersed Cu_3 clusters. Owing to the unique defect-rich structure of ND@G, the highly defective few-layer graphene outer-shells served as hosts for anchoring metal atoms (Fig. S1). Importantly, reduction at high temperature causes the agglomerate of metal atoms so that the atomically dispersed copper sites formed a three-atom cluster structure. Such a structure is probably favorable for catalyzing the decomposition of oxygen into reactive oxygen species (ROS).

In the XRD profiles (Fig. 2A), no diffraction peak associated with bulk Cu was observed on Cu-NPs/ND@G and Cu_3/ND@G, demonstrating that the Cu species were both highly dispersed on the ND@G surface without the presence of large Cu particles. The Raman spectra of Cu-NPs/ND@G and Cu_3/ND@G are shown in Fig. S3, and two distinct peaks appeared at approximately 1340 cm^{-1} and 1580 cm^{-1}, respectively, corresponding to the D and G bands. The I_D/I_G ratio of Cu_3/ND@G is 0.93, revealing that the instinct defect-rich structure on the ND@G surface. X-ray photoelectron spectroscopy (XPS) was subsequently employed to study the surface elemental composition and valence state of Cu-NPs/ND@G and Cu_3/ND@G (Fig. 2B). For Cu_3/ND@G, the Cu $2p^{3/2}$ peak appeared at 933 eV, situated between Cu^0/Cu^+ (932.7 eV) and Cu^{2+} (934.6 eV). Hence, the valence state of Cu_3 clusters is between Cu^0 and Cu^{2+}, due to the strong interaction between Cu_3 cluster and the ND@G support through formation of Cu-C bond. The Cu species in Cu-NPs/ND@G mainly exists in the form of metallic copper. It should be noted that the Cu LMM auger signal that is usually used to differentiate Cu^+ and Cu^0 was not obtained due to the poor quality of

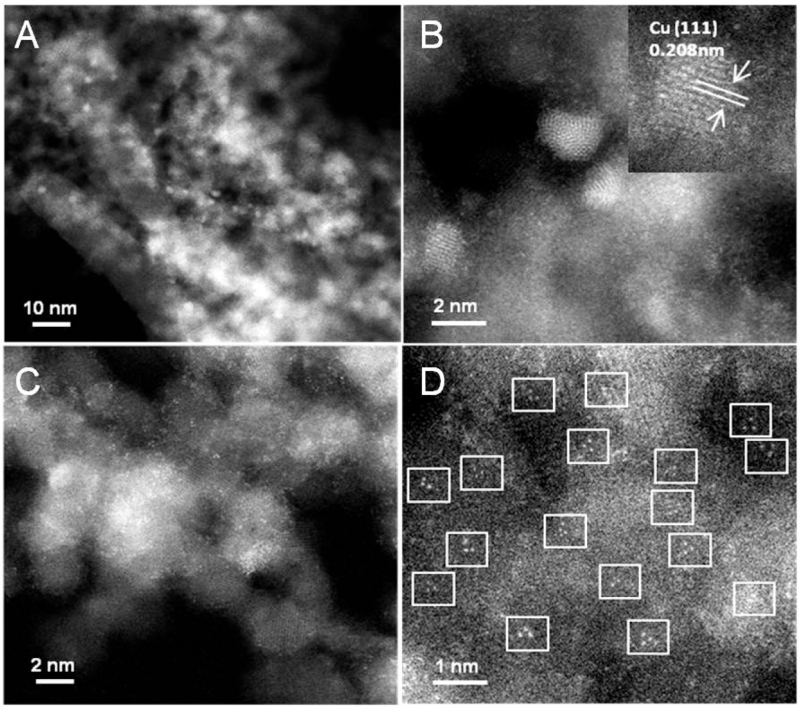

Fig. 1. Morphology characterization of Cu-NPs/ND@G and Cu_3/ND@G. AC-HAADF-STEM image of Cu-NPs/ND@G at low (A) and high (B) magnifications (inset is one single Cu nanoparticle with exposed (111) plane). AC-HAADF-STEM images of Cu_3/ND@G at low (C) and high (D) magnifications (typical fully exposed Cu_3 clusters are highlighted by the white rectangles in D).

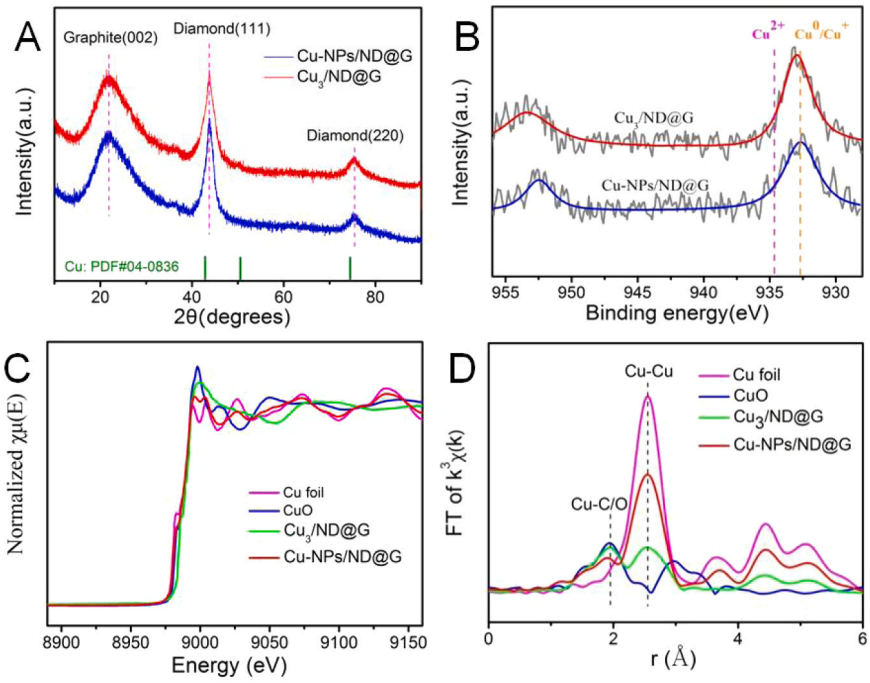

Fig. 2. Structure characterization of Cu-NPs/ND@G and Cu_3/ND@G. (A) XRD patterns of Cu-NPs/ND@G and Cu_3/ND@G. (B) XPS spectra of Cu-NPs/ND@G and Cu_3/ND@G. (C) XANES spectra and (D) Fourier transform (FT) of the Cu K-edge of Cu-NPs/ND@G, Cu_3/ND@G, CuO, and Cu foil.

the spectra.

X-ray absorption fine structure (XAFS) spectroscopy was used to characterize the fine atomic structure of Cu-NPs/ND@G and Cu_3/ND@G. X-ray absorption near edge structure (XANES) spectra indicate that the valence state of Cu in the Cu_3/ND@G is between 0 and + 2 in accordance with the chemical shift and the edge slope (see Fig. 2C). This is consistent with the XPS results (Fig. 2B). The XANES spectra of Cu-NPs/ND@G were close to that of Cu foil, suggesting that most of the Cu species in Cu-NPs/ND@G are in metallic state. Fourier-transformed (FT) k^2-weighted extended X-ray absorption fine structure (EXAFS) in R space was performed to elucidate the coordination environment of Cu atoms anchored on ND@G (Fig. 2D). Comparing with Cu foil, CuO and Cu-NPs/ND@G, the Cu_3/ND@G showed one main peak at 1.96 Å in the EXAFS spectra, corresponding to the first coordination shell of Cu-C/O. Besides the scattering of Cu-C at 1.96 Å, a major peak at 2.55 Å ascribed to Cu-Cu scattering was observed, indicating the formation of Cu cluster. The coordination number of Cu-Cu shell for Cu_3/ND@G is close to 2, evidencing that the Cu cluster is composed of three Cu atoms on average.

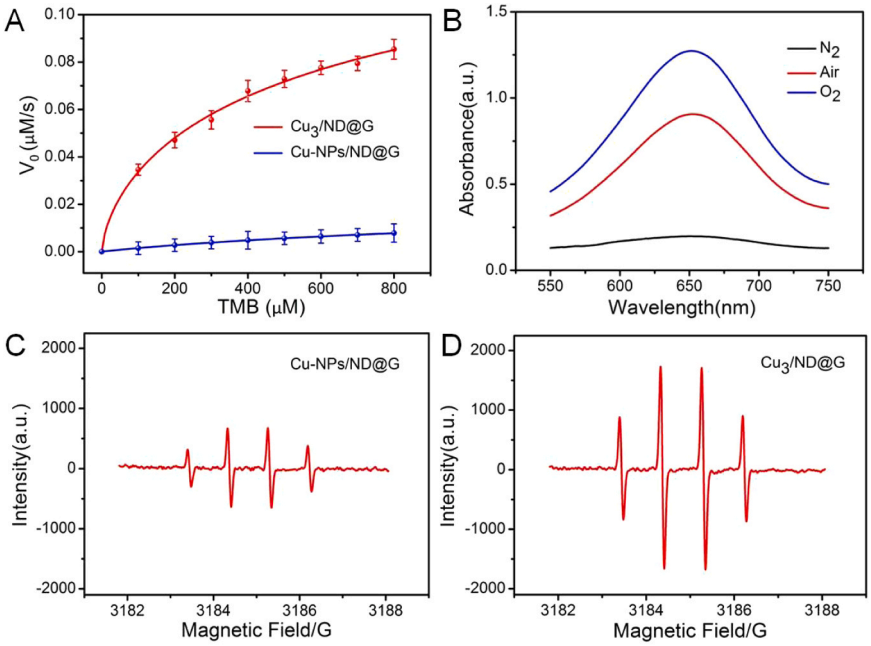

Fig. 3. Oxidase-like activity of Cu-NPs/ND@G and Cu_3/ND@G. (A) Typical Michaelis-Menten plots for Cu-NPs/ND@G and Cu_3/ND@G in the air-saturated NaAc buffer. (B) Ultraviolet-visible (UV–vis) absorption spectra of Cu_3/ND@G in the conditions of O_2-saturated, air-saturated, and N_2-saturated NaAc buffers. ESR spectra of DMPO/•OH adduct generated by Cu-NPs/ND@G (C) and Cu_3/ND@G (D) in air-saturated NaAc buffer solution (pH = 4.5).

For Cu-NPs/ND@G, the Cu-Cu peak dominated in Fig. 2D, revealing the presence of Cu-NPs. Moreover, the XPS measurement verified the existence of Cu-C in Cu_3/ND@G (Fig. S4). Least-square EXAFS fittings (Fig. S5, S6) were used to extract the structural parameters. The corresponding EXAFS fitting parameters are listed in Table S1.

3.2. The improved oxidase-like activity of Cu_3-cluster nanozyme

In order to systematically evaluate the oxidase-like activity of Cu_3/ND@G, we conducted a colorimetric experiment, in which 3, 3′, 5, 5′-tetramethylbenzidine (TMB) was employed as substrate. The Cu_3/ND@G in NaAc buffer medium (pH=4.5) at 37 ℃ can catalyze the oxidation of TMB in the presence of O_2, and the oxidized TMB (oxTMB) has a distinct absorption peak at 652 nm. We assessed the Michaelis-Menten kinetics of Cu_3/ND@G nanozyme in the present of varying concentrations of TMB (Fig. 3A). The results demonstrated that Cu_3/ND@G could effectively promote the dissociation of O_2 and enhance the catalytic oxidation of TMB. Furthermore, the Michaelis-Menten constant (K_m) of Cu_3/ND@G was determined to be 2.98 mM, suggesting the good affinity of Cu_3/ND@G toward TMB. In addition, the Cu_3/ND@G exhibit a high oxidase-like activity of 0.115 μM s^{-1}, which is 6 times higher than that of the Cu-NPs/ND@G. Notably, the catalytic rate constant (K_{cat}) of Cu_3/ND@G is 0.1474 s^{-1}, which is 15 times higher than that of the commercial Pt/C (Table S2). Moreover, the Cu_3/ND@G exhibit higher oxidase-like catalytic rate constant than those of previously reported copper-based oxidase mimics and copper single atom oxidase mimics [9, 13]. To explore the role of O_2 in the reaction, two control experiments were carried out in O_2 and N_2 saturated solutions, respectively (Fig. 3B). Compared to the absorbance at 652 nm of Cu_3/ND@G in the air-saturated buffer, the reaction rate of TMB oxidation catalyzed by Cu_3/ND@G increased significantly in O_2 saturation conditions, but decreased sharply under N_2 saturation conditions. Thus, the oxidation rate of TMB is highly dependent on O_2 concentration, revealing that the Cu_3/ND@G can catalyze the decomposition of O_2 into •OH. To further verify the oxidase-like activity of Cu_3/ND@G, the generated •OH was detected by the electron spin resonance (ESR) spectroscopy (see Fig. 3C and D). The ESR signal intensity of •OH in Cu_3/ND@G possesses a significant improvement when compared with that in Cu-NPs/ND@G, leading to the increased oxidase-like activity.

In order to investigate the mechanism of the oxidase-like activity of Cu_3/ND@G, we adopted density functional theory to predict the coordination structure and reaction mechanism of Cu_3/ND@G. We used Cu_3(OH) species doped into defect-rich (Cu_3(OH)/Gr) graphene to model Cu_3/ND@G, and use the Cu(111) surface to represent Cu-NPs/ND@G. Cu_3OH/Gr was recognized to be the active sites of Cu_3/ND@G due to its good thermodynamical stability and oxidation ability (see Fig. S7 and Table S3). The details of computational simulation methods can be found in the Methods section. Moreover, all the possible binding modes of different adsorbates on the catalytic surfaces are summarized in SI (Tables S4-6). As shown in Fig. 4, the detailed reaction path is composed of five thermochemical reaction steps [13]. First, the O_2 molecule is absorbed on Cu_3 active sites with adsorption energy of − 1.64 eV (i). This indicates that the Cu_3 cluster can strongly adsorb O_2, thus weakening the O-O bond. During the adsorption process, the Cu_3 cluster structure provides adjacent adsorption sites, thereby promoting the adsorption and cleavage of O_2. The lower adsorption energy (−0.86 eV) of Cu-NPs/ND@G leads to weak O_2 adsorption and thus weak activation of O-O bonds, which makes it less capable of catalyzing the dissociation of O_2. The OO* species can easily attract proton from solvent to generate the OOH* species (ii). Next, OOH* adsorbed on the Cu_3 site is dissociated into O* and •OH (iii). Then, the O* species attracts proton from solvent to generate the OH* species (iv). Finally, OH* desorbs from Cu_3 sites, leading to the formation of •OH (v). All elementary steps are exothermic, except the release of H_2O molecules (with an energy change of +0.29 eV). These results indicate that Cu_3/ND@G nanozyme can easily catalyze the dissociation of O_2 into •OH, in agreement with the experimentally observed high oxidase-like activity. The density functional theory calculations revealed that the synergetic interaction among adjacent Cu atoms in each cluster guarantees effective activation of O_2 and the easy desorption of •OH, resulting in increased oxidase-like activity by the Cu_3/ND@G.

3.3. The excellent antibacterial performance of Cu_3-cluster nanozyme

The plate count method was also used to evaluate the antibacterial activities of ND@G, Cu-NPs/ND@G and Cu_3/ND@G against *E. coli*. The antibacterial activities of the samples were shown in Fig. 5B-D. Compared with the control test (Fig. 5A), the Cu_3/ND@G showed the highest antibacterial activity. The parallel tests were provided in Fig. S8, and the antibacterial rate was shown in Fig. S9. We envisioned that the

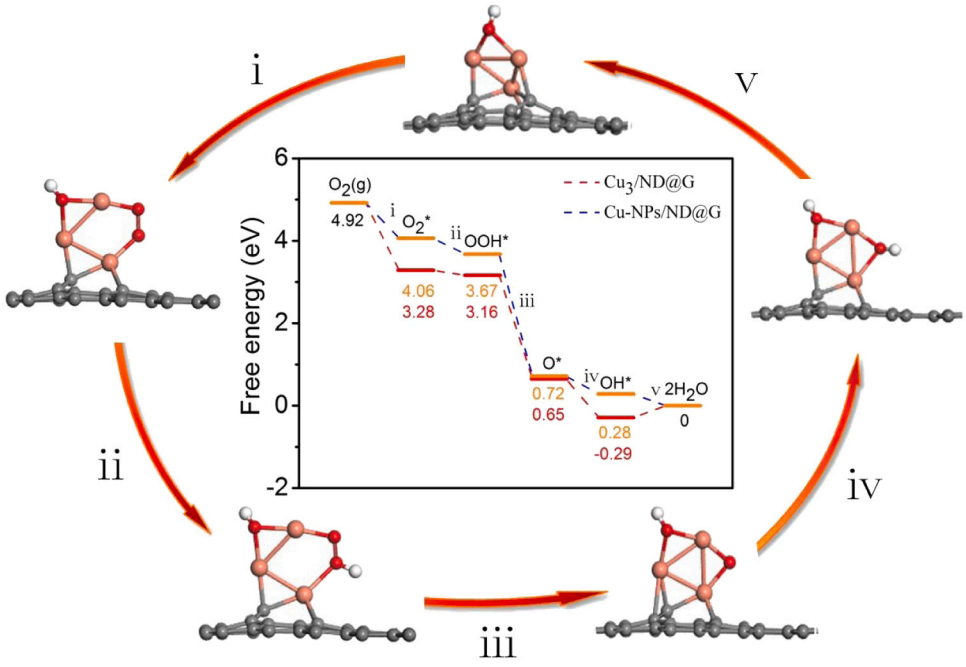

Fig. 4. Theoretical investigation of oxidase-like activity over Cu-NPs/ND@G and Cu_3/ND@G. The optimized adsorption configurations of various intermediates along the oxidase-like reaction path on Cu_3/ND@G and the free-energy diagram for the oxidase-like mechanism on Cu_3/ND@G and Cu-NPs/ND@G. The gray, brown, red and white balls represent C, Cu, O, and H atoms, respectively. (For interpretation of the references to colour in this figure legend, the reader is referred to the web version of this article.)

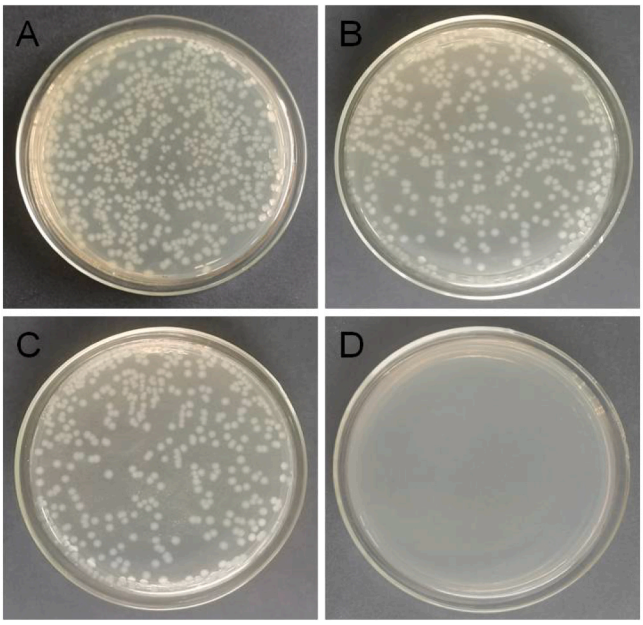

Fig. 5. Antibacterial performance of Cu-NPs/ND@G and Cu_3/ND@G. Growth inhibition assay: different materials and bacterial fluid coated on LB agar plate, cultivated with *E. coli* and treated with: (A) blank, (B) ND@G, (C) Cu-NPs/ND@G and (D) Cu_3/ND@G. Incubation condition: 37 °C and 24 h.

ability of Cu_3/ND@G to generate •OH from O_2 ultimately conferred an antibacterial effect. Meanwhile, the Cu_3/ND@G exhibited excellent capacity for bacterial capture, which enabled the nanozyme to obtain elevated ROS destruction. To further decipher the antibacterial behavior, the cell wall and membrane damage as well as the intracellular structural change in *E. coli* were examined by TEM after a 10 min treatment. As shown in Fig. S10, the cell walls of *E. coli* appeared to be damaged and disorganized after being treated with Cu-NPs/ND@G (B). The intracellular substrates leaked out of the cell and the cell morphology of bacteria completely lost after the treatment. Therefore, the as-prepared Cu_3/ND@G exhibited robust antibacterial properties. More importantly, TEM images (Fig. S10) further confirmed that the originally dispersed bacteria gathered at Cu_3/ND@G incubation, which was attributed to the capture effect of the large surface area of ND@G. Overall, the antibacterial experiment results and DFT calculations indicated that the Cu_3/ND@G with atomically dispersed and full exposed Cu_3 cluster presents robust antibacterial activity and shows its potential application in the field of antibacterial materials.

4. Conclusions

In summary, we fabricated an atomically dispersed and fully exposed Cu_3 cluster stabilized on defect-rich nanodiamond-graphene hybrid support (Cu_3/ND@G). The atomically dispersed and fully exposed Cu_3 cluster as active center significantly improved the oxidase-like activity of nanozyme, due to the easy decomposition of O_2 into reactive oxygen species (•OH). The DFT calculations revealed that the synergetic interaction among adjacent Cu atoms in each cluster resulted in increased oxidase-like activity. Importantly, the catalytic rate constant of as-prepared Cu_3/ND@G is much higher than those of previously reported copper-based oxidase mimics, copper single atom oxidase mimics and even the commercial Pt/C oxidase mimics. This study not only provides a new method to improve the oxidase-like activity of nanozyme, but also paves the way for extensive antibacterial research by the atomically dispersed and fully exposed metal-cluster.

CRediT authorship contribution statement

Hongyang Liu, Ding Ma, Lini Yang and **Lixin Xia** conceived the research. **Fanchi Meng** conducted material synthesis and carried out the performance test. **Mi Peng** conducted the X-ray absorption fine structure spectroscopic measurements and analyzed the data. **Yunlei Chen** and **Xiaodong Wen** performed the DFT calculations. **Xiangbin Cai** and **Ning Wang** contributed to the aberration-corrected high-angle annular dark-field scanning transmission electron microscopy. **Fei Hang, Xiao Liu** and **Tao Li** performed some of the experiments. The manuscript was primarily written by **Fanchi Meng**, **Yunlei Chen**, **Dequan Xiao**, **Hong Jiang, Hongyang Liu** and **Ding Ma.** All authors contributed to discussions and manuscript review.

Declaration of Competing Interest

The authors declare that they have no known competing financial interests or personal relationships that could have appeared to influence the work reported in this paper.

Acknowledgements

General: The XAS experiments were conducted in Shanghai Synchrotron Radiation Facility (SSRF).

Funding: The present work is supported by the National Natural Science Foundation of China (21773101, 21671089, 91845201, 21961160722, 22072162, 21725301, 21932002, 21821004), Liaoning Revitalization Talents Program (XLYC1807151, XLYC1907055), the National Key R&D Program of China (2016YFA0204100, 2017YFB0602200), Guangxi Key Laboratory of Information Materials (Guilin University of Electronic Technology), Project 201016-K. N.W. hereby acknowledges the funding support from the Research Grants Council of Hong Kong (Project Nos. C6021–14E, N_HKUST624/19 and 16306818). D.M. acknowledges support from the Tencent Foundation through the XPLORER PRIZE.

Appendix A. Supporting information

Supplementary data associated with this article can be found in the online version at doi:10.1016/j.apcatb.2021.120826.

References

[1] L. Gao, J. Zhuang, L. Nie, J. Zhang, Y. Zhang, N. Gu, T. Wang, J. Feng, D. Yang, S. Perrett, X. Yan, Intrinsic peroxidase-like activity of ferromagnetic nanoparticles, Nat. Nanotechnol. 2 (2007) 577–583.

[2] B. Xu, H. Wang, W. Wang, L. Gao, S. Li, X. Pan, H. Wang, H. Yang, X. Meng, Q. Wu, L. Zheng, S. Chen, X. Shi, K. Fan, X. Yan, H. Liu, A single-atom nanozyme for wound disinfection applications, Angew. Chem. Int. Ed. 58 (2019) 4911–4916.

[3] D. Wang, H. Wu, C. Wang, L. Gu, H. Chen, D. Jana, L. Feng, J. Liu, X. Wang, P. Xu, Z. Guo, Q. Chen, Y. Zhao, Self-assembled single-site nanozyme for tumor-specific amplified cascade enzymatic therapy, Angew. Chem. Int. Ed. 60 (2020) 3001–3007.

[4] H. Miao, D. Zhong, Z. Zhou, X. Yang, Papain-templated Cu nanoclusters: assaying and exhibiting dramatic antibacterial activity cooperating with H_2O_2, Nanoscale 7 (2015) 19066–19072.

[5] C. Liu, M. Zhang, H. Geng, P. Zhang, Z. Zheng, Y. Zhou, W. He, NIR enhanced peroxidase-like activity of Au@CeO_2 hybrid nanozyme by plasmon-induced hot electrons and photothermal effect for bacteria killing, Appl. Catal. B: Environ. 295 (2021), 120317.

[6] F. Cao, Y. Zhang, Y. Sun, Z. Wang, L. Zhang, Y. Huang, C. Liu, Z. Liu, J. Ren, X. Qu, Ultrasmall nanozymes isolated within porous carbonaceous frameworks for synergistic cancer therapy: enhanced oxidative damage and reduced energy supply, Chem. Mater. 30 (2018) 7831–7839.

[7] L. Wang, F. Gao, A. Wang, X. Chen, H. Li, X. Zhang, H. Zheng, R. Ji, B. Li, X. Yu, J. Liu, Z. Gu, F. Chen, C. Chen, Defect-rich adhesive molybdenum disulfide/rGO vertical heterostructures with enhanced nanozyme activity for smart bacterial killing Application, Adv. Mater. 32 (2020) 2005423.

[8] D. Wu, J. Li, S. Xu, Q. Xie, Y. Pan, X. Liu, R. Ma, H. Zheng, M. Gao, W. Wang, J. Li, X. Cai, F. Jaouen, R. Li, Engineering Fe-N doped graphene to mimic biological functions of NADPH oxidase in cells, J. Am. Chem. Soc. 142 (2020) 19602–19610.

[9] F. Li, N. Li, C. Xue, H. Wang, Q. Chang, H. Liu, J. Yang, S. Hu, A Cu_2O-CDs-Cu three component catalyst for boosting oxidase-like activity with hot electrons, Chem. Eng. J. 382 (2020), 122484.
[10] Y. Zhong, X. Liang, Z. He, W. Tan, J. Zhu, P. Yuan, R. Zhu, H. He, The constraints of transition metal substitutions (Ti, Cr, Mn, Co and Ni) in magnetite on its catalytic activity in heterogeneous Fenton and UV/Fenton reaction: From the perspective of hydroxyl radical generation, Appl. Catal. B: Environ. 150 (2014) 612–618.
[11] J. Wang, R. Huang, W. Qi, R. Su, B.P. Binks, Z. He, Construction of a bioinspired laccase-mimicking nanozyme for the degradation and detection of phenolic pollutants, Appl. Catal. B: Environ. 254 (2019) 452–462.
[12] H. Sun, Y. Zhou, J. Ren, X. Qu, Carbon nanozymes: enzymatic properties, catalytic mechanism, and applications, Angew. Chem. Int. Ed. 57 (2018) 9224–9237.
[13] L. Huang, J. Chen, L. Gan, J. Wang, S. Dong, Single-atom nanozymes, Sci. Adv. 5 (2019) eaav5490.
[14] W. Wu, L. Huang, E. Wang, S. Dong, Atomic engineering of single-atom nanozymes for enzyme-like catalysis, Chem. Sci. 11 (2020) 9741–9756.
[15] Y. Wu, J. Wu, L. Jiao, W. Xu, H. Wang, X. Wei, W. Gu, G. Ren, N. Zhang, Q. Zhang, L. Huang, L. Gu, C. Zhu, Cascade reaction system integrating single-atom nanozymes with abundant Cu sites for enhanced biosensing, Anal. Chem. 92 (2020) 3373–3379.
[16] L. Jiao, W. Xu, Y. Zhang, Y. Wu, W. Gu, X. Ge, B. Chen, C. Zhu, S. Guo, Boron-doped Fe-N-C single-atom nanozymes specifically boost peroxidase-like activity, Nano Today 35 (2020), 100971.
[17] N. Cheng, J.C. Li, D. Liu, Y. Lin, D. Du, Single-atom nanozyme based on nanoengineered Fe-N-C catalyst with superior peroxidase-like activity for ultrasensitive bioassays, Small 15 (2019) 1901485.
[18] C. Zhao, C. Xiong, X. Liu, M. Qiao, Z. Li, T. Yuan, J. Wang, Y. Qu, X. Wang, F. Zhou, Q. Xu, S. Wang, M. Chen, W. Wang, Y. Li, T. Yao, Y. Wu, Y. Li, Unraveling the enzyme-like activity of heterogeneous single atom catalyst, Chem. Commun. 55 (2019) 2285–2288.
[19] Y. Wang, Z. Zhang, G. Jia, L. Zheng, J. Zhao, X. Cui, Elucidating the mechanism of the structure-dependent enzymatic activity of Fe-N/C oxidase mimics, Chem. Commun. 55 (2019) 5271–5274.
[20] X. Zhang, M. Zhang, Y. Deng, M. Xu, L. Artiglia, W. Wen, R. Gao, B. Chen, S. Yao, X. Zhang, M. Peng, J. Yan, A. Li, Z. Jiang, X. Gao, S. Cao, C. Yang, A.J. Kropf, J. Shi, J. Xie, M. Bi, J.A. van Bokhoven, Y.W. Li, X. Wen, M. Flytzani-Stephanopoulos, C. Shi, W. Zhou, D. Ma, A stable low-temperature H_2-production catalyst by crowding Pt on α-MoC, Nature 89 (2021) 396–401.
[21] M. Peng, C. Dong, R. Gao, D. Xiao, H. Liu, D. Ma, Fully exposed cluster catalyst (FECC): toward rich surface sites and full atom utilization efficiency, ACS Cent. Sci. 7 (2020) 262–273.
[22] J. Zhang, Y. Deng, X. Cai, Y. Chen, M. Peng, Z. Jia, Z. Jiang, P. Ren, S. Yao, J. Xie, D. Xiao, X. Wen, N. Wang, H. Liu, D. Ma, Tin-assisted fully exposed platinum clusters stabilized on defect-rich graphene for dehydrogenation reaction, ACS Catal. 9 (2019) 5998–6005.
[23] F. Huang, Y. Deng, Y. Chen, X. Cai, M. Peng, Z. Jia, P. Ren, D. Xiao, X. Wen, N. Wang, H. Liu, D. Ma, Atomically dispersed Pd on nanodiamond/graphene hybrid for selective hydrogenation of acetylene, J. Am. Chem. Soc. 140 (2018) 13142–13146.
[24] F. Huang, Y. Deng, Y. Chen, X. Cai, M. Peng, Z. Jia, J. Xie, D. Xiao, X. Wen, N. Wang, Z. Jiang, H. Liu, D. Ma, Anchoring Cu_1 species over nanodiamond-graphene for semi-hydrogenation of acetylene, Nat. Commun. 10 (2019) 4431.
[25] S. Bhattacharyya, S.R. Ali, M. Venkateswarulu, P. Howlader, E. Zangrando, M. De, P.S. Mukherjee, Self-assembled Pd_{12} coordination cage as photoregulated oxidase-like nanozyme, J. Am. Chem. Soc. 142 (2020) 18981–18989.
[26] Y. Sun, P. Tian, D. Ding, Z. Yang, W. Wang, H. Xin, J. Xu, Y.F. Han, Revealing the active species of Cu-based catalysts for heterogeneous Fenton reaction, Appl. Catal. B: Environ. 258 (2019), 117985.
[27] R. Long, K. Mao, X. Ye, W. Yan, Y. Huang, J. Wang, Y. Fu, X. Wang, X. Wu, Y. Xie, Y. Xiong, Surface facet of palladium nanocrystals: a key parameter to the activation of molecular oxygen for organic catalysis and cancer treatment, J. Am. Chem. Soc. 135 (2013) 3200–3207.
[28] Z. Chen, Z. Wang, J. Ren, X. Qu, Enzyme mimicry for combating bacteria and biofilms, Acc. Chem. Res. 51 (2018) 789–799.
[29] F. Gao, T. Shao, Y. Yu, Y. Xiong, L. Yang, Surface-bound reactive oxygen species generating nanozymes for selective antibacterial action, Nat. Commun. 12 (2021) 745.
[30] L. Zhang, Z. Liu, Q. Deng, Y. Sang, K. Dong, J. Ren, X. Qu, Nature-inspired construction of MOF@COF nanozyme with active sites in tailored microenvironment and pseudopodia-like surface for enhanced bacterial inhibition, Angew. Chem. Int. Ed. 60 (2021) 3469–3474.
[31] G. Kresse, J. Furthmuller, Efficiency of ab-initio total energy calculations for metals and semiconductors using a plane-wave basis set, Comput. Mater. Sci. 6 (1996) 15–50.
[32] G. Kresse, J. Furthmuller, Efficient iterative schemes for ab initio total-energy calculations using a plane-wave basis set, Phys. Rev. B 54 (1996) 11169–11186.
[33] P.E. Blochl, Projector augmented-wave method, Phys. Rev. B 50 (1994) 17953–17979.
[34] G. Kresse, D. Joubert, From ultrasoft pseudopotentials to the projector augmented-wave method, Phys. Rev. B 59 (1999) 1758–1775.
[35] J.P. Perdew, K. Burke, M. Ernzerhof, Generalized gradient approximation made simple, Phys. Rev. Lett. 78 (1997).